ARTICLE TYPE

Enhanced Photoluminescence and Phosphorescence Properties of Red CaAlSiN₃:Eu²⁺ Phosphor via Simultaneous UV-NIR Stimulation

Jin Wang,[a] Haoran Zhang,[a] Bingfu Lei,*[a] Zhiguo Xia,[b] Hanwu Dong,[a] Yingliang Liu,*[a] Mingtao Zheng[a] and Yong Xiao[a]

Red-emitting CaAlSiN₃: Eu²⁺ phosphors with different doping content have been synthesized by solid-state reaction using calcium hydride as calcium source. The emergence of persistent 10 luminescence in CaAlSiN₃: Eu²⁺ was originated from electron traps introduced by the partial substitutions of O in N sites to form $O_N^•$ positive trap levels at low Eu²⁺ concentration. The broad thermoluminescence emission bands indicated multiple trap levels, in which the shallow traps were mainly responsible 15 for the red persistent luminescence; besides, the deep trap electrons could be efficiently released under extra NIR (980 nm) stimulation, resulting in enhanced photoluminescence and phosphorescence. It is expected that the enhanced emission under UV-NIR simultaneous excitation may be a promising technique 20 to investigate the trap distributions in optical energy storage materials.

1   Introduction

Persistent luminescence or long-lasting phosphorescence (LLP), as a research hotspot, has received much attention for the 25 significant values of academic researches and practical applications, such as security signs, emergency signage, dials, displays and decoration.[1] Compared to abundant quantity of the green and blue persistent luminescence compounds, inorganic phosphors emitting persistent luminescence from orange to near-30 infrared (NIR) spectral range are currently lacking. In recent years, the red or near-infrared (NIR) persistent luminescence nanoparticles, which are pre-excited by ultraviolet (UV) light before injection into biological tissues, have been extended to *in vivo* imaging system with the advantage to circumvent the 35 autofluorescence from living tissues.[2-4] Unfortunately, the afterglow intensity is relatively low due to size effect. There are some other reported red persistent phosphors, such as CaS: Eu²⁺, Tm³⁺,[5] and Y₂O₂S: Eu³⁺, Mg²⁺, Ti⁴⁺,[6] however, poor stability or toxicity restricts their applications. Therefore, novel red persistent 40 phosphors with suitable properties are expected.

As for the persistent mechanism, common understanding suggests that charge carrier traps are able to immobilize the carriers of electrons and holes (generated during UV irradiation process) transiently until thermally assisted release. Note that the 45 traps in most afterglow materials rarely presents as a single energy level but the overlap of multiple energy levels.[7, 8] As a result, the thermal stimulation at room temperature is not enough to detrap the electrons in deep traps, which can be regarded as power dissipation in some sense. Actually, NIR possessed higher 50 energy can effectively release the electrons in deep traps, producing kinds of luminous forms: photostimulated luminescence (PSL),[9] photostimulated persistent luminescence (PSPL),[10] and even up-converted persistent luminescence (UCPL).[11] Furthermore, if the stimulation time is long enough, 55 the NIR irradiation will exhaust the traps eventually. Motivation derived from above discussions, in this paper, we showed that the fluorescence and phosphorescence intensity were interestingly enhanced via UV-NIR simultaneous excitation, compared with only UV light excitation. It is expected that the enhanced 60 fluorescence under extra NIR stimulation may be a promising technique to improve luminous efficiency in some areas, like silicon solar cells and light conversion agricultural film.

Because of excellent thermal quenching property, high luminescent efficiency, great chemical and thermal stabilities, 65 CaAlSiN₃: Eu²⁺ phosphor has turned out to be excellent optical material for application in phosphor-converted w-LEDs.[12, 13] In recent years, reports about CaAlSiN₃: Eu²⁺ are most focused on investigating photoluminescence properties, optimizing the synthesis conditions and thermal quenching behaviors.[14-16] In 70 fact, defects, such as Ca vacancies and oxygen impurity, can also be introduced into the CaAlSiN₃ host compound and perform as traps centers which play an essential role for photo-energy storage in persistent materials, just as found in other nitride persistent phosphors.[17, 18] In this paper, high quality CaAlSiN₃: 75 Eu²⁺ phosphor was synthesized by solid-state reaction using calcium hydride as calcium source. We firstly observed exciting red persistent phenomenon and the CaAlSiN₃: 0.05%Eu²⁺ sample possessed persistence time as long as 45 min (≥ 0.32 mcd/m²). As mentioned, the samples exhibited obvious enhanced fluorescence 80 under UV-NIR excitation simultaneously, resulting from equilibrium of detrapping and retrapping of electrons in the traps. Additionally, the photoluminescence properties, oxygen content corresponding to electron traps, thermo-luminescence spectra analysis and some discussion have been performed in detail.

85

2   Experimental section

2.1   Materials and synthesis

A series of CaAlSiN$_3$: xEu^{2+} (x = 0.05%, 0.1%, 0.2%, 0.5%, 0.8%, 1%, 1.2%, 1.5% and 2%) phosphors were prepared by traditional high temperature solid-state reaction. CaH$_2$ (Aladdin, AR, Shanghai, China), AlN (Aladdin, AR, Shanghai, China), Si$_3$N$_4$ (SN-E10; UBE Industries, Tokyo, Japan) and Eu$_2$O$_3$ (99.99%) were used as the starting materials. After weighed and ground according to the given stoichiometric ratio, the mixtures were compressed into boron nitride crucibles and then were sintered at 1650 ^{o}C for 3 h in a radiofrequency induction furnace (CX-06, Genfu Co. Ltd., Suzhou, China) with a gas flow of 80 mL/min N$_2$ (99.999%). When temperature control program was finished, the samples were naturally cooled to room temperature in the furnace and ground again for next investigation.

2.2   Characterization

Crystal structure of the samples was analyzed by powder X-ray diffraction (XRD, XD-2X/M4600, Beijing Purkinje General Instruments Co., Ltd., Beijing, China) with Cu Kα radiation (λ = 1.5419 Å). The data was collected in a 2θ range from 20° to 70° with a scanning step of 0.02^o and a scanning rate of 4°/min. Morphology images were measured using a scanning electron microscope (SEM, XL-30, Phillips, Holland). The digital pictures of the samples are photographed using a digital camera (Canon EOS 40D, Japan). Photoluminescence (PL), photoluminescence excitation (PLE) and afterglow spectra were measured with a Hitachi F-7000 (Tokyo, Japan) spectrophotometer. Rhodamine B, a light diffuser, and a standard light source were used as references to correct the spectral distribution. Afterglow decay curve was obtained with a PR305 long afterglow instrument (Zhejiang University Sensing Instruments Co., Ltd., Hangzhou, China). TL behaviors were investigated by a microcomputer controlled TL dosimeters (FJ427–AL, Beijing Nuclear Instrument Factory, Beijing, China) with a fixed heating ratio 2 ^{o}C/s. Before TL measurement, the samples were pre-irradiated by 365 nm UV light for 5 min.

The UV-NIR simultaneous stimulation curves were recorded at the Hitachi 7000 spectrophotometer. The samples were loaded in the holder attached on the OXFORD OptistatDN to avoid the interference of any incident light. The holder was arranged at angles near 45° with respect to obtain the incident UV/NIR source and the entrance slit of the dispersing monochromator of the Hitachi 7000 spectrophotometer. Output power adjustable 405 nm UV laser and 980 nm NIR laser were used as stimulation sources, respectively. Suitable filters were used to correct for the baseline shift due to any stray light. Under the switch of UV/NIR stimulation off and on, the change of emission intensity was recorded.

3   Results and discussion

Earlier work carefully suggested that the compound formula Ca$_{1-\delta/2}$Al$_{1-\delta}$Si$_{1+\delta}$N$_3$ or CaAl$_{1-4\delta/3}$Si$_{1+\delta}$N$_3$ ($\delta \approx 0.3 \sim 0.4$) was more appropriate than the ideal CaAlSiN$_3$, on the basis of the observation of the ratio Al/Si $\neq$ 1 practically. [19] So it is easily understood that small amount of AlN is universally detected in the products when using the stoichiometric raw materials, like in

the case of CaAlSiN$_3$: Eu^{2+} [15] and CaAlSiN$_3$: Re^{3+} [20]. Herein, Fig. 1 shows the typical powder XRD patterns of CaAlSiN$_3$: xEu^{2+} (x = 0.05%, 0.2%, 0.5%, 1% and 2%). It is obvious that all the obtained samples are of single-phased CaAlSiN$_3$ (orthorhombic,

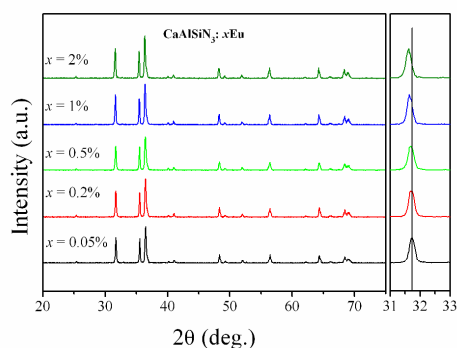**Fig. 1.** XRD patterns of CaAlSiN$_3$: xEu^{2+} (x = 0.05%, 0.2%, 0.5%, 1% and 2%) samples.

$Cmc2_1$), which also indicates that the Eu^{2+} ions do not induce any impurity or vitally change the host structure. Given that the ionic radius of Eu^{2+} (r = 1.17 Å) is similar to that of Ca^{2+} (r = 1.00 Å), but much larger than Si^{4+} (r = 0.40 Å) and Al^{3+} (r = 0.54 Å), the Eu^{2+} ions are expected to occupy the Ca sites in the CaAlSiN$_3$ host lattice. Therefore, with increasing concentration of dopant ions, small shifts toward lower 2θ value in the diffraction peaks are observed due to the lattice expansion.
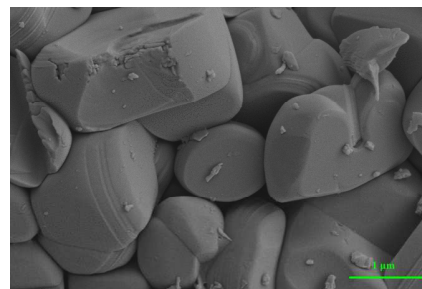

Fig. 2. SEM image of CaAlSiN$_3$: 0.05%Eu^{2+} sample.

Fig. 2 gives the SEM photograph of the CaAlSiN$_3$: 0.05%Eu^{2+} sample. As seen, the as-prepared phosphor is composed of irregular particles with narrow size distribution around 1 ~ 3 μm in diameter. The blunt surface of the main grains, accompanied by the existence of much smaller ones among them, is attributed to the grinding operation after the samples were cooled to temperature in the furnace. In our experimental range, the size and morphologies of the phosphors seem to be independent of the dopant concentration of Eu^{2+} ions.
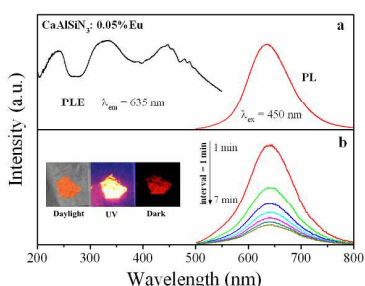
Fig. 3. PLE, PL (a) and afterglow emission (b) spectra of CaAlSiN$_3$: 0.05%Eu^{2+} phosphor. The lower inset is the photographs of the sample in daylight, under 365 nm UV excitation and in the dark, respectively.

It is well-known that Eu^{2+} doped CaAlSiN$_3$ phosphor, as a promising red phosphor for the fabrication of warm w-LEDs, has a broad excitation band ranging from UV to visible part, especially with the ability to be effectively excited by blue (around 450 nm) LED chip. The excitation and emission spectra of CaAlSiN$_3$: 0.05%Eu^{2+} are presented in Fig. 3a. The excitation spectrum monitored at 635 nm consists of three main bands, peaking at 240, 330 and 450 nm, respectively. The first band is ascribed to the transition between the valance and conduction bands of the CaAlSiN$_3$ host. Yet, the latter two bands peaking at 330 and 450 nm are responsible to the electric transitions from the ground state to the different crystal field splitting bands of the excited 5d states of Eu^{2+}. It is noted that the 5d levels of Eu^{2+}, not shielded from the outside environment, are split under different ligand field strength and the number of split levels is determined by the local symmetry around Eu^{2+} ions.[21] For these reasons the 5d levels of Eu^{2+} can be separated as T$_2$ and E levels due to a slightly distorted T_d site symmetry in a EuN$_4$ tetrahedron.[14] The emission spectrum (λ_{ex} = 450 nm) of CaAlSiN$_3$: 0.05%Eu^{2+} shows a symmetrically broad emission band with a half peak width of 91.6 nm and peaks at 635 nm, which is assigned to the allowed 4f^{6}5d → 4f^7 transition of Eu^{2+} ions. Since the luminescence centers experience high nephelauxetic effect and large crystal field splitting effect in CaAlSiN$_3$ host lattice, the peak position is located at relatively long wavelength side even in low concentration Eu^{2+} doping sample.
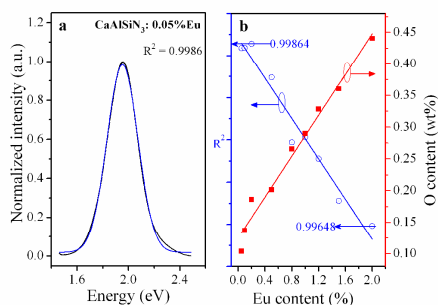

Fig. 4. Emission fitted curves by Gaussian method of CaAlSiN$_3$: 0.05%Eu^{2+} (a); and Dependence of R-square values (blue line) and oxygen content (red line) on Eu^{2+} content (b).

In the structure of CaAlSiN$_3$: Eu^{2+}, there is only one crystallographic Ca^{2+} site that can be substituted by the Eu^{2+} activator. Based on this, one peak originating from the site is supposed to appear as a symmetrical emission band. However,

two distinct Gaussian peaks were observed in CaAl$_x$Si$_{(7-3x)/4}$N$_3$: Eu^{2+} and Ca(Al/Si)$_2$N$_2$(N$_{1-x}$O$_x$): Eu^{2+}, as a result of the change of the Al/Si molar ratio around Eu^{2+} and the formation of EuN$_3$O because of partial substitution N by O, respectively.[22, 23] It can be concluded that the emission of Eu^{2+} ions is seriously dependent on the local structure of the host lattice or exactly on the crystal environment around Eu^{2+} ions. Certainly, the main aim of above modifications in CaAlSiN$_3$ host lattice is to achieve higher color rendering for use in LEDs applications, after all, the CaAlSiN$_3$: Eu^{2+} phosphors process quite deep red emission. In our present case, the series of various Eu^{2+} concentration doped CaAlSiN$_3$ samples show single symmetrically emission bands with the goodness of Gaussian fit (R-square) ranging between 0.99864 and 0.99648, as shown in Fig. 4a & b. As found in all nitride compounds, a small amount of oxygen is inevitably detected. In the typical sample CaAlSiN$_3$: 2%Eu^{2+}, the oxygen content is successfully suppressed to 0.44 wt%, better than 0.6 wt% by using self-propagating high-temperature synthesis.[14] Note that the oxygen content rises similarly in proportion with the increasing concentration of Eu^{2+} (see Fig. 4b), it indicates that the contamination of oxygen is likely to originate from the Eu$_2$O$_3$ or/and other commercial raw materials. Meantime, the effect of the increasing oxygen content is ultimately reflected in the decreasing R-square values, resulting from slight change of crystal environment around Eu^{2+} ions owing to the O incorporation into EuN$_4$ to from EuN$_3$O. Although the oxygen contamination is undesired for the greedy pursuit of pure productions, the trace oxygen impurity can take the place of N^{3-} to form $O_N^{\bullet}$ ($O^{2-} \xrightarrow{N^{3-}} O_N^{\bullet}$) positive trap levels, which are quite important for further use in producing afterglow.[17, 24] Indeed, the persistent luminescence is observed in all the obtained samples. Fig. 3b exhibits afterglow emission spectra and the images of CaAlSiN$_3$: 0.05%Eu^{2+} under daylight, UV irradiation and in the dark, respectively. Direct visual observation of strong red emission is performed with the illumination of 365 nm UV light. After UV excitation, obvious persistent luminescence is presented in dark environment. The afterglow spectra are similar in shape and peak position compared to the fluorescence spectrum under the 450 nm excitation, indicating that the persistent luminescence of CaAlSiN$_3$: Eu^{2+} corresponds to the 4f^{6}5d→4f^7 transition of Eu^{2+} ions; that is to say, the radiation centers in both cases are same.
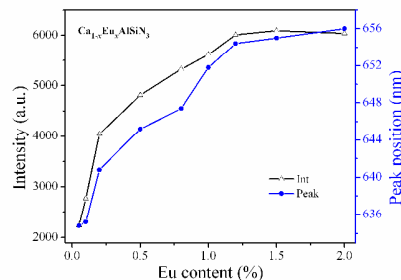

Fig. 5. Dependence of emission intensity and peak position of CaAlSiN$_3$: xEu^{2+} phosphors on Eu^{2+} content.

Fig. 5 depicts the dependence of emission intensity and peak positions of the CaAlSiN$_3$: xEu^{2+} (x = 0.05%, 0.1%, 0.2%, 0.5%, 0.8%, 1%, 1.2%, 1.5% and 2%) on Eu^{2+} ion concentration. With

increasing Eu^{2+} content, the emission peak wavelength increases from 635 nm to 656 nm (633.5 cm^{-1} redshift), and the emission intensity is maximized at the Eu^{2+} concentration at $x = 1.5\%$ which is almost consistent with the first report, where the quenching concentration is 1.6%.[25] Dexter pointed out that the quenching phenomenon is mainly attributed to the energy transfer (non-radiative and radiative energy transfer) between two types of the activator by electric dipole-quadrupole interaction or electron spin effect.[26] Besides, the redshift behavior can also be blamed on the site-to-site energy transfer.[27] As mentioned above, the inhomogeneous distribution of Al and Si ions at an identical crystallographic site, along with the partial substitution of N by O, generates a number of different local structures around the Eu^{2+} activator, whose effect have shown in the slightly decreasing R-square values for Gaussian fit of the PL emission spectra (see Fig. 4b). The higher activator concentration decreases the inter-activator distance of Eu^{2+} ions residing at different local environments. Consequentially, there is more chance for the site-to-site energy transfer to lower energy side.
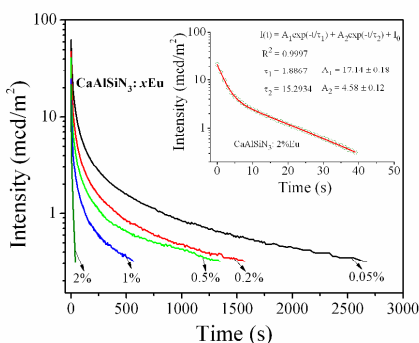

Fig. 6. Afterglow decay curves of CaAlSiN₃: xEu^{2+} phosphors after 10 min irradiation with a Xe arc lamp at 1000 lux.

The most interesting result of our present work is that obvious red persistent luminescence was observed in the CaAlSiN₃: Eu^{2+} phosphor. Fig. 6 shows the afterglow decay curves of the samples with different Eu^{2+} concentration after 10 min irradiation with a Xe arc lamp at 1000 lux, the dash-line is the limit of light perception of dark-adapted human eyes (0.32 mcd/m^2). The persistence time from sample CaAlSiN₃: $0.05\%Eu^{2+}$ is around 45 min. In general, persistent luminescent materials with a low concentration of the dopant and codopant ions own the better afterglow performance.[18, 28, 29] This is also confirmed by Fig. 6, where the afterglow duration and initial afterglow intensity decrease with the Eu^{2+} concentration increasing, in which the persistence time falls to 40 s in CaAlSiN₃: $2\%Eu^{2+}$ and the initial afterglow intensity reduces from 63.2, 47.9, 32.8, 24.5 to 14.7 mcd/m^2, respectively. The concentration quenching behaviour can be attributed to increasing possibility of interactions between traps when the content of doping ions exceeds the critical concentration, resulting in more easily movement of charge carriers from one trap to another. However, the exactly quenching concentration has not been ascertained because the quality of raw materials needs to weigh is too low to control accurately under our experimental conditions. In addition, it is found that the decay curves can be well fitted by frequently used bi-exponential function

$$I(t) = I_0 + A_1 \exp(-t / \tau_1) + A_2 \exp(-t / \tau_2) \qquad (1)$$

where I is the phosphorescence intensity at time t and I_0 is the background luminescence intensity, A_1 and A_2 are constants while τ_1 and τ_2 are the decay times for the exponential components, respectively. The afterglow intensity exhibits a very fast decay at first and then slowly, corresponding to the first exponential firstly and then the second exponential when the decay time is longer, respectively. This type of behavior is typical for most persistent materials.[17, 29] In the case of CaAlSiN₃: $2\%Eu^{2+}$ (see inset of Fig. 6), values of τ_1 and τ_2 are 1.89 s and 15.29 s, respectively. As for CaAlSiN₃: $0.05\%Eu^{2+}$, they become 128.19 s and 11.99 s, respectively, indicating that the CaAlSiN₃: $0.05\%Eu^{2+}$ sample takes more time to reduce the afterglow intensity to low level partly because the lower Eu^{2+} content doped-CaAlSiN₃ have larger initial afterglow intensity.

As mentioned, persistent luminescence relies upon transient storage of the radiation energy in charge carriers traps, immediately followed by the slow detrapping and radiative recombination of the carriers (electrons and holes) after ceasing the irradiation. Specific to the origins of traps in CaAlSiN₃: Eu^{2+}, Eu^{2+} at the Ca^{2+} site will work as a hole-trapping center $Eu_{Ca}^{\times}$ ($Eu^{2+} \xrightarrow{Ca^{2+}} Eu_{Ca}^{\times}$) because it is more electropositive than Ca^{2+};[18] and the formation of Ca vacancies ($Ca^{2+} \rightarrow V_{Ca}^{''}$), which can also perform as hole traps, is inevitable when high-temperature treatment is applied in sintered process. Additionally,
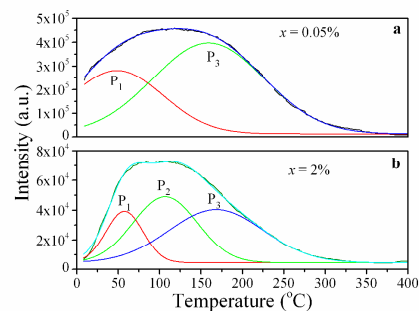

Fig. 7. TL glow curves and corresponding Gaussian peaks of CaAlSiN₃: $0.05\%Eu^{2+}$ (a) and CaAlSiN₃: $2\%Eu^{2+}$ (b).

Table 1. Experimental parameters and TL data for different samples.

Sample	P_1 (ºC)	P_2 (ºC)	P_3 (ºC)	TL Int (a.u.)	R^2
0.05%	48.6	−	159.2	4.6×10^5	0.9994
0.2%	52.9	−	153.8	2.7×10^5	0.9985
0.5%	65.0	103.2	168.3	1.7×10^5	0.9968
1%	61.0	115.9	181.5	8.7×10^4	0.9972
2%	57.5	106.8	168.4	7.3×10^4	0.9988

the trace oxygen impurity can take the place of N^{3-} to form $O_N^{\cdot}$ positive trap levels, which can sever as electron traps to intercept excited electrons for further use in producing afterglow.[24] Whatever origin a hole trap may dominate, TL of Eu^{2+} results from the recombination of electrons and holes at a Eu^{2+} center. To date, TL glows cure is one of the main used methods to provide information about traps, like trap depth and its concentration corresponding to the TL peak position and intensity, respectively. In order to investigate the traps in

CaAlSiN$_3$: Eu^{2+}, its TL spectra were recorded after 5 min UV (365 nm) irradiation. The glow curves of all samples show broad TL bands, indicating the multiple trap levels exist in CaAlSiN$_3$: Eu^{2+} phosphors. Fig. 7 gives the TL glow curves of the typical
5 samples with x = 0.05% and 2%, accompanied by two (referred to as P$_1$ and P$_3$) and three (referred to as P$_1$, P$_2$ and P$_3$) deconvoluted TL peaks, respectively. The detailed TL data (peak positions, total TL intensity and R-square of fitted curves) for samples with various doping concentrations are listed in Table 1. On the one
10 hand, as seen, the TL glow curves show concentration dependence: the TL intensity decreases with increasing europium content, between which the maximum difference in intensity is near to an order of magnitude. This behavior is not hard to understand because the TL glow curve shows a similar
15 concentration quenching effect due to the interaction of neighboring defect traps.[30] On the other hand, the deconvoluted peaks can be divided into three approximate trap levels, namely, P$_1$ (48.6 ~ 65.0 ^{o}C), P$_2$ (103.2 ~ 115.9 ^{o}C) and P$_3$ (153.8 ~ 181.5 ^{o}C). In spite of the fact that the artificial graduations of traps
20 based temperature difference are not very rigorous, these affirm the existence of multiple trap levels (shallow and deep traps) to some extent.

The TL experimental data presented above shows the TL bands cover broad temperature ranges, from 20 to 300 ^{o}C. In practice,
25 efficient persistent luminescence observed at room temperature is most often associated with TL bands occurring between 300 and 420 K to let the carriers be detrapped slowly by thermal energy.[31] Based on the locations of trap levels P$_1$ and P$_2$, the samples with Eu^{2+} at below 2% doping level did possess persistent
30 luminescence phenomenon after high energy excitation (see Fig. 6). Meanwhile taking into account concentration quenching in TL intensity, the reason for the lower Eu^{2+} ions content doped samples owning better afterglow performance is because the distribution of traps in low content doped samples is more
35 intensive. As to the trap level P$_3$, it is too deep for persistent luminescence to release the captured carriers under only room temperature stimulation. And the deep traps can retrap part of the electrons released by shallow traps immediately at room temperature, which will reduce the persistent luminescence
40 property. However, it is worth noting that the presence of deep stable traps able to immobilize the carriers permanently at room temperature is exactly what is required for efficient storage phosphors, which have already found important applications as photostimulated materials.[30]
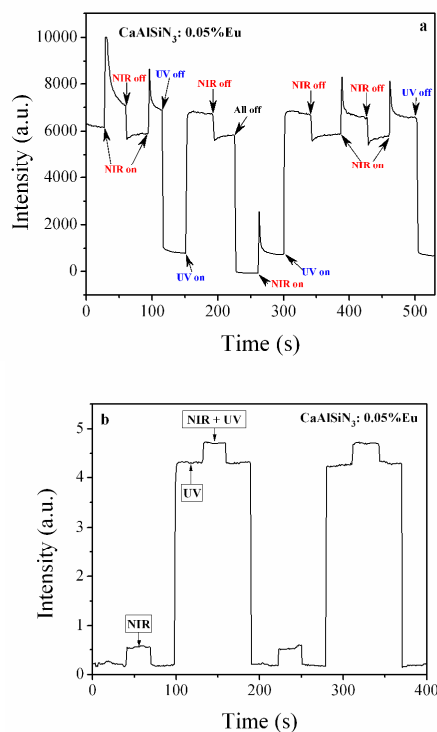

Fig. 8. Variation of emission intensity under the switch of UV/NIR stimulation off and on in CaAlSiN$_3$: 0.05%Eu^{2+}, after 10 min UV (365 nm) pre-irradiation (a) and pre-treatment of 24 h darkness (b).
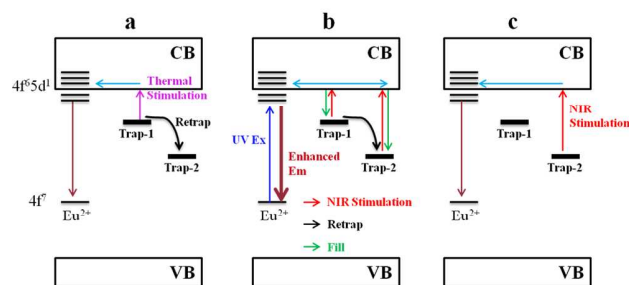

Fig. 9. Schematic representation of electron transfer under natural decay (a), simultaneous UV-NIR stimulation (b) and single NIR stimulation (c).

Given that the deep traps (P$_3$ > 150 ^{o}C) fastened part of UV excitation energy, so the ambient thermal energy is too low to
55 release trapped electrons in deep levels. In part, the immobilization of deep trapped electrons reduces subsequent afterglow performance after the removal of excitation source and even decreases initial fluorescence intensity until the deep traps are full, both of which mean power dissipation. It is worth noting
60 that the NIR, possessed higher energy, can effectively release the electrons in deep traps, producing kinds of luminous forms: photostimulated luminescence (PSL), photostimulated persistent luminescence (PSPL) and even up-converted persistent luminescence (UCPL).[9-11] Furthermore, if the NIR stimulation
65 time is long enough, the deep traps will be emptied eventually. Then, inspiration of simultaneous UV-NIR stimulation strikes, and it is expected that enhanced fluorescence and phosphorescence can be achieved under simultaneous UV-NIR

stimulation due to equilibrium of detrapping and retrapping of electrons in traps.

Motivated by this method, the emission intensity of CaAlSiN$_3$: 0.05%Eu^{2+} was measured with the switch of UV/NIR stimulation on and off, and it exhibited obvious changes, as shown in Fig. 8a. Several cyclic operations were given. Initially, the 405 nm UV irradiation is kept eradiating on the sample. When extra NIR photostimulation was added to the sample, the fluorescence intensity increases to higher value and then shows a decay trend. Followed by NIR stimulation off, the intensity takes some time to recover to stable level. However, as the NIR stimulation turns on again, the intensity become quite strong again, even higher than that at the moment when former NIR is off. Finally, after all UV and NIR stimulation are off, the re-addition of only NIR irradiation promotes photostimulated persistent luminescence, whereas no phenomenon of stronger intensity is observed when UV is on again. Interestingly, above performances can reappear at the same procedure. Based on the experimental data, we proposed schematic representation of electron transfer under different stimulation modes, as shown in Fig. 9. When the persistent luminescence decays in natural way, electrons release from the shallow traps (i.e. Trap-1) and then are transferred to luminescence centers through conduction band (see Fig. 9a). Under the irradiation of 405 nm UV laser, the excitation populates the 4f^{6}5d^1 states of Eu^{2+}, followed by the filling of shallow traps and deep traps (i.e. Trap-2) (see Fig. 9b). Then, the stimulation of a 980 nm NIR laser promotes the depopulation of electrons in shallow traps and part detrapping of electrons in deep traps, showing as a photostimulated persistent luminescence process. Note that simultaneous UV-NIR stimulation corresponds to equilibrium of detrapping and retrapping of electrons in traps and result in the 4f^{6}5d^1→4f^7 emission of Eu^{2+} at the same time, this is why this operation performs to enhance the photoluminescence and phosphorescence intensity ultimately. Of course, due to the constant UV irradiation, the empty traps will be filled again. This can be identified by Fig. 8a, namely, all the intensities under only UV excitation must take some time to recover to stable level after the NIR stimulation is off.

Meanwhile, it is hard to ignore that part of electrons released from shallow traps can be retrapped by deep traps, which happened in all process (Fig. 9a & b). Actually, the stronger photostimulated luminescence intensity is also partly attributed to the effect of electrons retrapped by deep traps. In order to further confirm this idea, Fig. 8b also shows the variation of emission intensity under the switch of UV/NIR stimulation off and on in CaAlSiN$_3$: 0.05%. The difference is that the sample is of pre-treatment of 24 h in darkness. As the NIR stimulation is on, the photostimulated luminescence, only originating from the detrapping of electrons in deep traps, is still observed (as schematically shown in Fig. 9c). But the phenomenon of stronger intensity is gone when the 980 nm laser just opens because the pre-treatment of darkness have emptied the shallow traps. Besides, the recovery process of intensity after the NIR stimulation was off failed to emerge again, this fact suggests that the recovery of intensity above (see Fig. 8a) is indeed the result of traps filling instead of instrument response.

4 Conclusion

As a summarization, we have successfully synthesized a series of high-quality CaAlSiN$_3$: Eu^{2+} phosphors and investigated their luminescence properties. The obtained samples were single phases without AlN impurity and showed symmetric emission band with quenching concentration at about 1.5 at. %. The high performances profited from quite low oxygen contamination content, but crucial in producing persistent luminescence (as long as 45 min in CaAlSiN$_3$: 0.05%Eu^{2+}). The afterglow duration time and intensity exhibited concentration dependence behaviors due to lower trap density in high Eu^{2+} content samples, verified by the TL analysis. It was also found that traps in CaAlSiN$_3$: Eu^{2+} possessed multiple trap levels: the shallow traps responsible for persistent luminescence and the deep traps able to immobilize the carriers permanently at room temperature. Under UV-NIR simultaneous excitation, the release of electrons from traps reached equilibrium of detrapping and retrapping. From the application point of view, the enhanced photoluminescence and phosphorescence via simultaneous UV-NIR stimulation may be a promising technique to improve luminous efficiency in some areas or as a tool to investigate the trap distributions in optical energy storage materials.

Notes and references

^{a}College of Science, South China Agricultural University, Guangzhou 510642, P. R. China.
^{b}School of Materials Sciences and Engineering, University of Science and Technology Beijing, Beijing,100083, China
E-mail: *tleibf@scau.edu.cn* (B. Lei), *tliuyl@163.com* (Y. Liu).
Tel. : +86-20-85280323; Fax. : +86-20-85285026

1   W. M. Yen, S. Shionoya and H. Yamamoto, *Practical applications of phosphors*, CRC Press, Boca Raton, 2007.
2   Q. L. de Chermont, C. Chaneac, J. Seguin, F. Pelle, S. Maitrejean, J. P. Jolivet, D. Gourier, M. Bessodes and D. Scherman, *Proc. Natl. Acad. Sci. USA*, 2007, **104**, 9266.
3   T. Maldiney, G. Sraiki, B. Viana, D. Gourier, C. Richard, D. Scherman, M. Bessodes, K. Van den Eeckhout, D. Poelman and P. F. Smet, *Opt. Mater. Express*, 2012, **2**, 261.
4   T. Maldiney, A. Bessière, J. Seguin, E. Teston, S. K. Sharma, B. Viana, A. J. J. Bos, P. Dorenbos, M. Bessodes, D. Gourier, D. Scherman and C. Richard, *Nat. Mater.*, 2014, **13**, 418.
5   D. D. Jia, W. Y. Jia, D. R. Evans, W. M. Dennis, H. M. Liu, J. Zhu, and W. M. Yen, *J. Appl. Phys*., 2000, **88**, 3402.
6   X. X. Wang, Z. T. Zhang, Z. L. Tang and Y. H. Lin, *Mater. Chem. Phys*., 2003, **88**, 1.
7   K. Van den Eeckhout, D. Poelman and P. F. Smet, *Materials*, 2013, **6**, 2789.
8   K. Van den Eeckhout, D. Poelman and P. F. Smet, *Materials*, 2013, **3**, 2536.
9   W. Jia, H. Yuan, S. Holmstrom, H. Liu and W. M. Yen, *L. Lumin*.,

1999, **83-4**, 465.

10　F. Liu, W. Z. Yan, Y.-J. Chuang, Z. P. Zhen, J. Xie and Z. W. Pan, *Sci. Rep.*, 2013, **3**, 1554.

11　F. Liu, Y. J. Liang and Z. W. Pan, *Phys. Rev. Lett.*, 2014, **113**, 177401.

12　R.-J. Xie and H. T. Hintzen, *J. Am. Ceram. Soc.*, 2013, **96**, 665.

13　M. Zeuner, S. Pagano and W. Schnick, *Angew. Chem. Int. Ed.*, 2011, **50**, 7754.

14　X. Q. Piao, K. Machida, T. Horikawa, H. Hanzawa, Y. Shimomura and N. Kijima, *Chem. Mater.*, 2007, **19**, 4592.

15　T. Suehiro, R.-J. Xie and N. Hirosaki, *Ind. Eng. Chem. Res.*, 2014, **53**, 2713.

16　S.-S. Wang, W.-T. Chen, Y. Li, J. Wang, H.-S. Sheu and R.-S. Liu, *J. Am. Chem. Soc.*, 2013, **135**, 12504.

17　H. R. Zhang, M. T. Zheng, B. F. Lei, Y. Xiao, H. W. Dong, Y. L. Liu, X. T. Liu, J. J. Deng, J. W. Deng and Z. L. Huang, *ECS Solid State Lett.*, 2013, **2**, R16.

18　B. F. Lei, K. Machida, T. Horikawa, H. Hanzawa, N. Kijima, Y. Shimomura and H. Yamamoto, *J. Electrochem. Soc.*, 2010, **157**, J196.

19　Y. Q. Li, N. Hirosaki, R. J. Xie, T. Takeda and M. Mitomo, *Chem. Mater.*, 2008, **20**, 6704.

20　Z. J. Zhang, O. M. Kate, A. Delsing, E. Van der Kolk, P. H. L. Notten, P. Dorenbos, J. T. Zhao and H. T. Hintzen, *J. Mater. Chem.*, 2012, **22**, 9813.

21　W. M. Yen, S. Shionoya and H. Yamamoto, *Fundamentals of phosphors*, CRC Press, Boca Raton, 2007

22　Y. W. Jung, B. Lee, S. P. Singh and K.-S. Sohn, *Opt. Express*, 2010, **18**, 17805.

23　T. Wang, P. Zheng, X. L. Liu, H. F. Chen, S. S. Yang and Q. L. Liu, *J. Electrochem. Soc.*, 2014, **161**, H25.

24　Y. Miyamoto, H. Kato, Y. Honna, H. Yamamoto and K. Ohmi, *J. Electrochem. Soc.*, 2009, **156**, J235.

25　K. Uheda, N. Hirosaki and H. Yamamoto, *Phys. Stat. Sol. A*, 2006, **203**, 2712.

26　D. L. Dexter, *J. Chem. Phys.*, 1953, **21**, 836.

27　S. J. Lee and K.-S. Sohn, *Opt. Lett.*, 2010, **35,** 1004.

28　X. H. Xu, Q. L. He and L. T. Yan, *J. Alloy. Compd.*, 2013, **574**, 22.

29　X. Liu, J. H. Zhang, X. Zhang, Z. D. Hao, J. Qiao and X. L. Dong, *Opt. Lett.*, 2013, **38**, 148.

30　J. Trojan-Piegza, J. Niittykoski, J. Holsa and E. Zych, *Chem. Mater.*, 2008, **20**, 2252.

31　A. Lecointre, A. Bessière, A. J. J. Bos, P. Dorenbos, B. Viana and S. Jacquart, *J. Phys. Chem. C*, 2011, **115**, 4217.

Enhanced Photoluminescence and Phosphorescence Properties of Red CaAlSiN$_3$:Eu^{2+} Phosphor via Simultaneous UV-NIR Stimulation
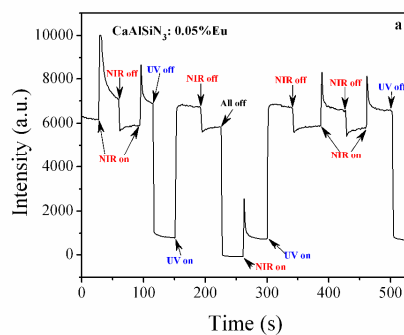*Jin Wang, Haoran Zhang, Bingfu Lei [*], and Yingliang Liu*, et al.*

Table of Contents(TOC):

Enhanced Photoluminescence and Phosphorescence Properties of Red CaAlSiN$_3$:Eu^{2+}

Phosphor via Simultaneous UV-NIR Stimulation

Jin Wang, Haoran Zhang, Bingfu Lei*, Zhiguo Xia, Hanwu Dong, Yingliang Liu, Mingtao Zheng, Yong Xiao

 Enhanced emission was observed under simultaneous UV-NIR stimulation due to equilibrium of detrapping and retrapping of electrons in traps.